Thermal light subwavelength diffraction using positive and negative correlations

Mingjie Sun (孙鸣捷)[1,*], Xingdan He (何兴丹)[1], Mingfei Li (李明飞)[2,3], and Ling'an Wu (吴令安)[2]

[1]*Department of Opto-Electronic Engineering, Beihang University, Beijing 100191, China*
[2]*Laboratory of Optical Physics, Institute of Physics and Beijing National Laboratory for Condensed Matter Physics, Chinese Academy of Sciences, Beijing 100190, China*
[3]*Quantum Engineering Research Center, Beijing Institute of Aerospace Control Devices, China Aerospace, Beijing 100094, China*
**Corresponding author: Mingjie.Sun@buaa.edu.cn*

Received October 23, 2015; accepted February 4, 2016; posted online March 21, 2016

Ghost imaging and diffraction, inspired by the Hanbury Brown and Twiss effect, have potential in both classical and quantum optics regimes on account of their nonlocal characteristics and subwavelength resolution capability, and therefore have aroused particular interest. By extending the correspondence imaging scheme, we utilize the positive and negative intensity correlations in diffraction and perform subwavelength diffraction with pseudo-thermal light. In the experiment, a subwavelength ($\lambda/2$) resolution and a better signal-to-noise ratio (10.3% improvement) are simultaneously achieved. The scheme can be utilized as a complement to the existing ghost imaging scheme to improve image quality.

OCIS codes: 030.0030, 030.4280, 050.0050, 110.1650, 110.6150.
doi: 10.3788/COL201614.040301.

The Hanbury Brown and Twiss (HBT) effect is a classical intensity correlation phenomenon that was first employed in an intensity interferometer to measure the angular size of distant stars. It has much better resolution and visibility than the Michelson stellar interferometer because it measures the second-order, intensity–intensity correlation of two separate intensity detectors rather than the first-order, field-field correlation[1]. Though the effect was originally explained by HBT with the classical wave theory, it aroused a debate on the classical or quantum nature of the phenomenon, which has lasted to this day. Despite this, the HBT effect is widely exploited in both the classical and quantum regimes, and has led to many important developments in quantum optics, particle physics, and practical applications, among which ghost imaging[2–11] and ghost diffraction[12–14] have aroused particular interest in both fundamental optics and imaging technology.

Ghost imaging, first implemented with entangled light[2], has promising potential in many applications on account of its apparently nonlocal characteristics and subwavelength resolution capability[15,16], as well as its relatively simple implementation with classical thermal light[5–7,17–19]. The second-order intensity–intensity correlation for thermal light only has a maximum Michelson contrast (also known as visibility, defined as $(I_{\max}-I_{\min})/(I_{\max}+I_{\min})$) of 33%. Many schemes have been demonstrated to improve its contrast[20–25], including a scheme that achieved 100% correlation[26]. However, according to the definition of Michelson contrast, its value can always reach 100% after a unity-based normalization. In practical measurement, different noise levels will lead to different signal-to-noise ratios (SNRs) of the experimental results, even though the contrasts can all reach 100%. Therefore, the SNR provides a better criterion for image or pattern quality in experiments and applications.

Just like ghost imaging, ghost diffraction was first demonstrated using spontaneous parametric down-conversion, and at the time was attributed to the quantum entanglement of photons[12,27]. Then, ghost diffraction was performed using thermal light[13], and subwavelength resolution performance was predicted[28] and realized[14,29], even with two independent pseudothermal sources[30].

In this Letter, by extending a previously developed technique called correspondence ghost imaging[31,32], we demonstrate that it is possible to achieve a better SNR (10.3% improvement) and subwavelength ($\lambda/2$) resolution simultaneously in a thermal light diffraction experiment. We first extend the concept of the positive and negative correlations and employ them in diffraction. An experiment on thermal light subwavelength diffraction and its results are then presented, followed by a discussion and our conclusions. All correlations mentioned in this Letter are in the spatial regime.

A schematic of the diffraction setup is shown in Fig. 1. A thermal light field passes through a double slit and then is divided by a 50–50 beam splitter into Paths 1 and 2. In Path 1, the point-like Detector 1 is scanned along one direction in the transverse plane and measures the field intensity $I_1(x_1)$ as a function of the transverse position x_1. In Path 2, the point-like Detector 2 is scanned along the opposite direction in the transverse plane and

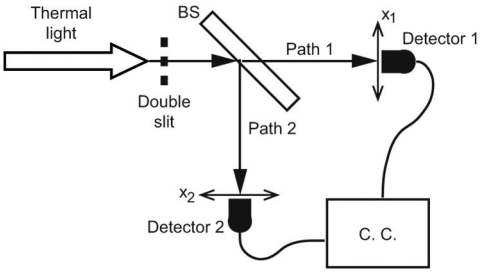

Fig. 1. Schematic of setup to measure diffraction. BS, 50–50 beam splitter; C.C., coincidence counter.

measures the field intensity $I_2(x_2)$ as a function of the transverse position x_2. The time averaged intensities at these two detectors are denoted as $\overline{I_1}(x_1) = \langle I_1(x_1)\rangle$ and $\overline{I_2}(x_2) = \langle I_2(x_2)\rangle$, respectively.

If one detector, e.g., Detector 1, is fixed at x_0, while the other, Detector 2, is scanned along axis X_2, then a classical diffraction pattern can be obtained by performing an intensity correlation with $I_1(x_0)$ and $I_2(x_2)$[14] using

$$g_{CI}^{(2)} = \frac{\langle I_1(x_0)I_2(x_2)\rangle}{\langle I_1(x_0)I_2(x_2)\rangle} = 1 + \frac{\mathrm{cov}(I_1(x_0)I_2(x_2))}{\langle I_1(x_0)\rangle\langle I_2(x_2)\rangle}, \quad (1)$$

where $\langle\ldots\rangle$ is the temporal mean, and cov is the covariance between $I_1(x_0)$ and $I_2(x_2)$, defined as $\mathrm{cov}(I_1(x_0)I_2(x_2)) = \langle(I_1(x_0) - \langle I_1(x_0)\rangle)(I_2(x_2) - \langle I_2(x_2)\rangle)\rangle$.

If the two detectors are scanned along axes X_1 and X_2, respectively, in opposite directions, a subwavelength diffraction can be obtained[14] by performing the second-order intensity correlation with $I_1(x_1)$ and $I_2(x_2)$ using

$$g_{SI}^{(2)} = \frac{\langle I_1(x)I_2(-x)\rangle}{\langle I_1(x)\rangle\langle I_2(-x)\rangle} = 1 + \frac{\mathrm{cov}(I_1(x)I_2(-x))}{\langle I_1(x)\rangle\langle I_2(-x)\rangle}, \quad (2)$$

where $x = x_1 = -x_2$. Because there is a constant term or background in this intensity–intensity correlation function, the contrast has a maximum of 33%. To enhance the contrast of the intensity correlation, the fluctuation correlation is frequently utilized as

$$g_{\mathrm{SIF}}^{(2)} = \frac{\langle I_1(x)I_2(-x)\rangle}{(\overline{I_1}(x)\overline{I_2}(-x))} - 1 = \frac{\langle \mathrm{cov}(I_1(x)I_2(-x))\rangle}{\langle I_1(x)\rangle\langle I_2(-x)\rangle}, \quad (3)$$

which is of the same mathematical form as the intensity correlation after unity-based normalization.

In our previous work[31,32], the data recorded by Detector 1 was separated into two sets according to whether the intensity was above or below the mean value of the data. Using these two sets of data, we were able to get the positive and negative correlation results. We shall now show how the positive and negative correlation is enhanced when the intensity values in both paths are initially separated into positive and negative groups.

In the setup of Fig. 1, because of the thermal fluctuations, the outputs of both detectors will fluctuate around their average intensities. We now separate $I_1(x)$ and $I_2(-x)$ into two groups according to the following conditions:

$$I_1 = \begin{cases} I_{1+}(x), & I_1(x) \geq \bar{I}_1(x) \\ I_{1-}(x), & I_1(x) < \bar{I}_1(x) \end{cases},$$
$$I_2(-x) = \begin{cases} I_{2+}(-x), & I_2(-x) \geq \bar{I}_2(-x) \\ I_{2-}(-x), & I_2(-x) < \bar{I}_2(-x) \end{cases}. \quad (4)$$

For a given point on the plane of Detector 2, there are four possible intensity correlations, as follows:

$$\langle I_{1+}I_{2+}\rangle = \frac{1}{4}\langle(\bar{I}_1 + \Delta I_{1+})(\bar{I}_2 + \Delta I_{2+})\rangle$$
$$= \frac{1}{4}(\bar{I}_1\bar{I}_2 + \bar{I}_1\langle\Delta I_{2+}\rangle + \langle\Delta I_{1+}\rangle\bar{I}_2 + \langle\Delta I_{1+}\Delta I_{2+}\rangle), \quad (5)$$

$$\langle I_{1+}I_{2-}\rangle = \frac{1}{4}\langle(\bar{I}_1 + \Delta I_{1+})(\bar{I}_2 + \Delta I_{2-})\rangle$$
$$= \frac{1}{4}(\bar{I}_1\bar{I}_2 + \bar{I}_1\langle\Delta I_{2-}\rangle + \langle\Delta I_{1+}\rangle\bar{I}_2 + \langle\Delta I_{1+}\Delta I_{2-}\rangle), \quad (6)$$

$$\langle I_{1-}I_{2+}\rangle = \frac{1}{4}\langle(\bar{I}_1 + \Delta I_{1-})(\bar{I}_2 + \Delta I_{2+})\rangle$$
$$= \frac{1}{4}(\bar{I}_1\bar{I}_2 + \bar{I}_1\langle\Delta I_{2+}\rangle + \langle\Delta I_{1-}\rangle\bar{I}_2 + \langle\Delta I_{1-}\Delta I_{2+}\rangle), \quad (7)$$

$$\langle I_{1-}I_{2-}\rangle = \frac{1}{4}\langle(\bar{I}_1 + \Delta I_{1-})(\bar{I}_2 + \Delta I_{2-})\rangle$$
$$= \frac{1}{4}(\bar{I}_1\bar{I}_2 + \bar{I}_1\langle\Delta I_{2-}\rangle + \langle\Delta I_{1-}\rangle\bar{I}_2 + \langle\Delta I_{1-}\Delta I_{2-}\rangle). \quad (8)$$

In these equations, (x) and $(-x)$ are omitted for simplicity, and ΔI_1 and ΔI_2 are the intensity fluctuations of Detectors 1 and 2, respectively. The factor 1/4 in these equations implies that there is only a 1/4 chance for each case to happen in one coinciding event. Assuming the number of measurements is large enough and the detectors measure all possible values in the intensity fluctuation range, then we will have $\langle\Delta I_{1+}\rangle + \langle\Delta I_{1-}\rangle = \langle\Delta I_{2+}\rangle + \langle\Delta I_{2-}\rangle = 0$, $\langle\Delta I_{1+}\Delta I_{2+}\rangle = \langle\Delta I_{1-}\Delta I_{2-}\rangle$ and $\langle\Delta I_{1+}\Delta I_{2-}\rangle = \langle\Delta I_{1-}\Delta I_{2+}\rangle$. Adding Eqs. (5) to (8) and Eqs. (6) and (7), along with the assumed approximation, gives

$$g_{\mathrm{SIP}}^{(2)} = 0.5 + \frac{\langle\Delta I_{1+}I_{2+}\rangle}{2\overline{I_1}\,\overline{I_2}}, \quad (9)$$

$$g_{\mathrm{SIN}}^{(2)} = 0.5 + \frac{\langle\Delta I_{1-}I_{2+}\rangle}{2\overline{I_1}\,\overline{I_2}}. \quad (10)$$

Since $\langle\Delta I_{1+}I_{2+}\rangle$ are positive and $\langle\Delta I_{1-}I_{2+}\rangle$ are negative, Eqs. (9) and (10) are defined as the positive and negative second-order intensity correlations, respectively.

This calculation shows that if the intensity fluctuations are within the dynamic range of the detectors and the sampling time is long enough, then the positive and negative second-order intensity correlations will both have the same background of 0.5. However, since $\langle \Delta I_{1+} I_{2+} \rangle > 0$ and $\langle \Delta I_{1-} I_{2+} \rangle < 0$, the positive correlation has a small peak above the background, while the negative one has a small dip below. Furthermore, subtracting Eq. (10) from Eq. (9) gives the cross-correlation of the positive and negative correlations:

$$g^{(2)}_{\mathrm{SI(P\text{-}N)}} = \frac{(\langle \Delta I_{1+} \Delta I_{2+} \rangle - \langle \Delta I_{1-} \Delta I_{2+} \rangle)}{2\overline{I_1}\,\overline{I_2}}. \qquad (11)$$

Based on the assumption that the dynamic range of the detectors and the sampling number are large enough, the positive and negative correlation have symmetrical noise. Therefore, this P–N correlation has a zero background, theoretically. In practice, the subtraction will always cancel part of the noise and thus enhance the SNR of the correlation. An experiment to verify this hypothesis is described below.

Figure 2 shows the experimental setup of the diffraction using the positive and negative correlations with thermal light. A laser beam at $\lambda = 532$ nm, emitted from a continuous-wave diode-pumped laser, goes through a polarizer and a ground glass plate rotating at a speed of 3 cycles/min to form a pseudothermal light source. A double slit (0.5 mm width and 1 mm separation, center to center) is placed directly after the ground glass. The light is then separated into two paths by a 50–50 beam splitter and received by two charge-coupled device (CCD) cameras (Imaging Source DMK 31BU03), which are placed 170 mm away from the double slit ($L_1 = L_2 = 170$ mm in Fig. 2). Both cameras, consisting of 1024 pixels × 768 pixels with a pixel size of 4.65 μm (spacing included), are operated at a rate of 20 Hz with an exposure time of 0.1 ms, taking a total number of 20000 sampling frames. Furthermore, the CCDs are triggered simultaneously by an external signal generator and two BNC cables of the same length. Therefore, we assumed the measured correlations have zero time difference and 100% temporal correlation.

Upon receiving the data from the CCDs, the classic diffraction pattern (Fig. 3(a)) is obtained by selecting the

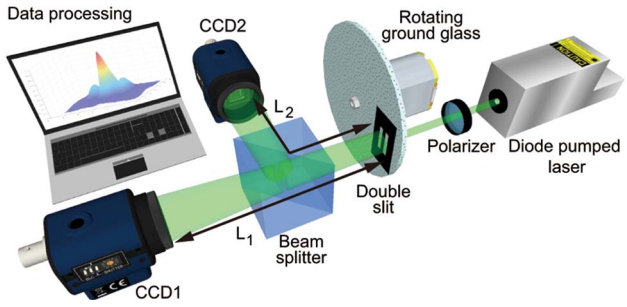

Fig. 2. Experimental setup for measuring positive and negative correlations in diffraction.

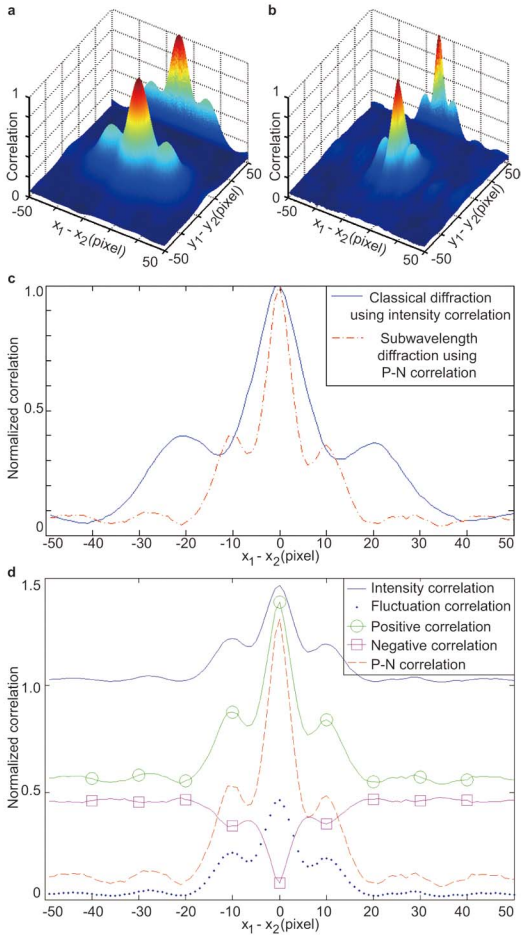

Fig. 3. Experimental results of classical and subwavelength diffraction with thermal light using positive and negative correlatiosn. (a) Classical diffraction obtained with intensity correlation. (b) Subwavelength diffraction obtained with P–N correlation. (c) Comparison of classical and subwavelength diffraction in one dimension. (d) Subwavelength diffraction obtained with different correlations.

intensity value of the center pixel in CCD1 and all the intensity values of the different pixels in CCD2 of all the sampling frames and applying Eq. (1). The subwavelength diffraction pattern (Fig. 3(b)) is obtained by using all intensity values of both CCDs of all the sampling frames and applying Eq. (11). Furthermore, different correlations of subwavelength diffraction (Fig. 3(d)) can be obtained by applying Eqs. (3) and (9)–(11). Table 1 shows the SNRs and noise mean square errors (MSEs) of the classic diffraction and subwavelength diffraction with different correlation functions. The SNRs are calculated from the equation

$$\mathrm{SNR} = 1/\delta g^{(2)}, \qquad (12)$$

where δ is the standard deviation, representing the noise level, $g^{(2)}$ is the certain correlation function under investigation, and the signal peak intensity of the correlation function is normalized to 1. The MSEs are calculated from the equation

Table 1. SNRs and MSEs of the Diffraction Patterns

SNR/MSE	Classical	Subwavelength
Intensity correlation	49.94/0.000401	65.05/0.000236
P–N correlation	56.36/0.000315	71.76/0.000194

$$\mathrm{MSE} = \frac{1}{mn}\sum_{i=1}^{m}\sum_{j=1}^{n}\left(g^{(2)}(i,j) - \overline{g^{(2)}}\right)^2, \tag{13}$$

where m and n are the two-dimensional pixel lengths of the results, and $\overline{g^{(2)}}$ is the mean value of $g^{(2)}$. It is worth mentioning that Fig. 3 shows the data of the center 100 pixels × 100 pixels, while the SNRs listed in Table 1 are calculated using the diffraction pattern results of the full 1024 pixels × 768 pixels. From these results, we can make the following observation:

1. Figures 3(a) and 3(c) show that the distance between adjacent peaks of the classical diffraction is ∼20 pixels (93 μm). This agrees well with the diffraction fringe period calculated by $\frac{\lambda D}{d} \approx 90.4$ μm, where $D = L_1 = L_2 = 170$ mm is the distance from the double slit to the detectors, and $d = 1$ mm is the separation of the double slit. Figures 3(b) and 3(c) show that the distance between adjacent peaks of the subwavelength diffraction is ∼10 pixels (46.5 μm). This agrees well with the diffraction fringe period calculated with a half of the light wavelength $(\lambda/2)D/d \approx 45.2$ μm.
2. Figure 3(d) shows that the positive (green circle) and negative (pink square) correlations have symmetrical forms and backgrounds around 0.5, which agrees with the theoretical analysis before.
3. To quantize the diffraction pattern quality, the SNRs and MSEs of the diffraction patterns obtained by the intensity correlation and P–N correlation are calculated using Eqs. (12) and (13), respectively (listed in Table 1). Better qualities are obtained in both the classic and subwavelength diffraction cases with P–N correlation, which gives relative SNR improvements of 12.8% and 10.3%, respectively. Therefore, in the thermal light diffraction experiment utilizing the positive and negative correlations, a better SNR (10.3% improvement) and a subwavelength ($\lambda/2$) resolution are simultaneously achieved.

The positive and negative correlation scheme in this article does not increase the Michelson contrast of the diffraction patterns because all patterns have 100% contrast after unity-based normalization. However, as we have described before, the noise induced in the experiments can be cancelled to some extent by utilizing the positive and negative correlation scheme, therefore giving results with better SNRs. It is worth mentioning that when the two detectors scan along the same direction, subwavelength diffraction is possible using either an entangled tow-photon light source[12] or a classic thermal light source[33].

In conclusion, we extend the positive and negative correlation scheme proposed in Refs. [31,32], and apply it to diffraction. The experimental results demonstrate that by utilizing this method, a diffraction pattern with a better SNR (10.3% improvement) and a subwavelength ($\lambda/2$) resolution can be achieved simultaneously. More importantly, this scheme is performed after the data acquisition and does not require any change in experimental setup; thus, it can be used as a complement to the existing ghost imaging schemes to achieve better image quality[34,35].

This work was supported by the National Basic Research Program of China (No. 2010CB922904), the National Natural Science Foundation of China (No. 61307021), and the China Scholarship Council (No. 201306025016)

References

1. R. H. Brown and R. Q. Twiss, Nature **177**, 27 (1956).
2. T. B. Pittman, Y. H. Shih, D. V. Strekalov, and A. V. Sergienko, Phys. Rev. A **52**, R3429 (1995).
3. R. S. Bennink, S. J. Bentley, and R. W. Boyd, Phys. Rev. Lett. **89**, 113601 (2002).
4. R. S. Bennink, S. J. Bentley, R. W. Boyd, and J. C. Howell, Phys. Rev. Lett. **92**, 033601 (2004).
5. A. Gatti, E. Brambilla, M. Bache, and L. A. Lugiato, Phys. Rev. Lett. **93**, 093602 (2004).
6. G. Scarcelli, A. Valencia, and Y. H. Shih, Europhys. Lett. **68**, 618 (2004).
7. D. Zhang, Y. H. Zhai, L. A. Wu, and X. H. Chen, Opt. Lett. **30**, 2354 (2005).
8. R. S. Aspden, D. S. Tascal, R. W. Boyd, and M. J. Padgett, New J. Phys. **15**, 073032 (2013).
9. B. Q. Sun, M. P. Edgar, R. Bowman, L. E. Vittert, S. Welsh, A. Bowman, and M. J. Padgett, Science **340**, 844 (2013).
10. X. Xu, E. Li, X. Shen, and S. Han, Chin. Opt. Lett. **13**, 071101 (2015).
11. X. Li, C. Deng, M. Chen, W. Gong, and S. Han, Photon. Res. **3**, 153 (2015).
12. M. D'Angelo, M. V. Chekhova, and Y. H. Shih, Phys. Rev. Lett. **87**, 013602 (2001).
13. F. Ferri, D. Magatti, A. Gatti, M. Bache, E. Brambilla, and L. A. Lugiato, Phys. Rev. Lett. **94**, 183602 (2005).
14. J. Xiong, D. Z. Cao, F. Huang, H. G. Li, X. J. Sun, and K. G. Wang, Phys. Rev Lett. **94**, 173601 (2005).
15. Y. H. Shih, IEEE J. Sel. Top. Quant. **13**, 1016 (2007).
16. J. H. Shapiro and R. W. Boyd, Quantum Inf. Process **11**, 949 (2012).
17. Y. H. Zhai, X. H. Chen, D. Zhang, and L. A. Wu, Phys. Rev. A **72**, 043805 (2005).
18. D. Z. Cao, J. Xiong, and K. Wang, Phys. Rev. A **71**, 013801 (2005).
19. X. H. Chen, Q. Liu, K. H. Luo, and L. A. Wu, Opt. Lett. **34**, 695 (2009).
20. I. N. Agafonov, M. V. Chekhova, T. S. Iskhakov, and A. N. Penin, Phys. Rev. A **77**, 053801 (2008).
21. D. Z. Cao, J. Xiong, S. H. Zhang, L. F. Lin, L. Gao, and K. G. Wang, Appl. Phys. Lett. **92**, 201102 (2008).
22. X. H. Chen, I. N. Agafonov, K. H. Luo, Q. Liu, R. Xian, M. V. Chekhova, and L. A. Wu, Opt. Lett. **35**, 1166 (2010).
23. Q. Liu, X. H. Chen, K. H. Luo, W. Wu, and L. A. Wu, Phys. Rev. A **79**, 053844 (2009).
24. P. Hong, J. Liu, and G. Zhang, Phys. Rev. A **86**, 013807 (2012).
25. A. Zhang, W. Li, L. Zhao, H. Ye, Y. Liu, X. Wei, and Z. Wang, Chin. Opt. Lett. **12**, 052701 (2014).
26. H. Chen, T. Peng, and Y. H. Shih, Phys. Rev. A **88**, 023808 (2013).

27. D. Z. Cao, Z. Li, Y. H. Zhai, and K. Wang, Euro. Phys. J. D **33**, 137 (2005).
28. K. G. Wang and D. Z. Cao, Phys. Rev. A **70**, 041801 (2004).
29. D. Z. Cao and K. Wang, Phys. Lett. A **333**, 23 (2004).
30. Y. H. Zhai, X. H. Chen, and L. A. Wu, Phys. Rev. A **74**, 053807 (2006).
31. L. A. Wu and K. H. Luo, AIP Conf. Proc. **1384**, 223 (2011).
32. K. H. Luo, B. Q. Huang, W. M. Zheng, and L. A. Wu, Chin. Phys. Lett. **29**, 074216 (2012).
33. D. Z. Cao, G. J. Ge, and K. G. Wang, Appl. Phys. Lett. **97**, 051105 (2010).
34. M. J. Sun, M. F. Li, and L. A. Wu, Appl. Opt. **54**, 7494 (2015).
35. X. Yao, X. Liu, W. Yu, and G. Zhai, Chin. Opt. Lett. **13**, 010301 (2015).